

Designer macrocyclic organo-peptide hybrids inhibit the interaction between p53 and HDM2/X by accommodating a functional α -helix†

Cite this: *Chem. Commun.*, 2014, 50, 5027

Received 14th February 2014,
Accepted 18th March 2014

Jessica M. Smith, John R. Frost and Rudi Fasan*

DOI: 10.1039/c4cc01199f

www.rsc.org/chemcomm

We report the design of side-chain-to-tail linked organo-peptide hybrids incorporating an α -helical protein-binding motif. Using this strategy, macrocyclic inhibitors of the p53:HDM2 interaction displaying dual specificity against the HDMX homolog as well as increased proteolytic stability could be obtained.

The development of agents for selective modulation of protein-protein interactions (PPIs) constitutes a prominent goal in drug discovery and chemical biology.¹ Since PPIs are often mediated by well defined secondary structural elements, a promising strategy in this area has involved the stabilization or mimicry of these motifs *via* compact molecular scaffolds.² Reflecting their abundance in protein structures, α -helices are often encountered at the interface of protein-protein complexes.³ Accordingly, a number of strategies have been developed for stabilization of α -helical peptides,⁴ which include the use of hydrogen bond surrogates⁵ as well as of a variety of inter-side-chain linkages such as disulfide,⁶ lactam,⁷ thioether⁸ or triazole⁹ bridges, 'hydrocarbon staples',¹⁰ and cysteine cross-linking moieties.¹¹

We recently reported strategies for the synthesis of macrocyclic organo-peptide hybrids (MOrPHs) *via* the chemo- and regioselective ligation of bifunctional synthetic precursors to genetically encoded precursor polypeptides (*e.g.* Fig. 1A).¹² A key feature of this new class of peptide-based macrocycles is their modular architecture, as given by the diverse non-peptidic and peptidic moieties amenable to incorporation into these scaffolds.^{12a,c} As part of ongoing studies directed at evaluating MOrPHs as disruptors of biomedically relevant PPIs, we were interested in assessing the potential of these macrocyclic scaffolds to accommodate, and possibly, stabilize a functional α -helical motif. In this work, we describe the successful implementation of this idea through the design and development of α -helical MOrPHs that can effectively disrupt the interaction between the tumor suppressor p53 and the oncoproteins HDM2 and HDMX.

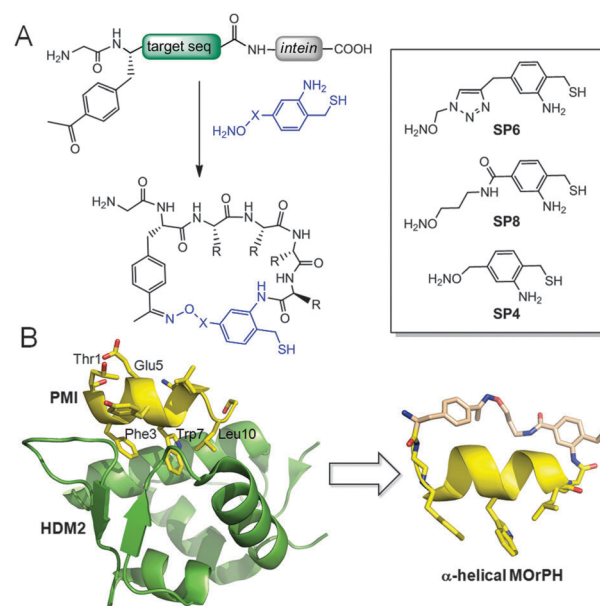


Fig. 1 (A) MOrPH macrocyclization strategy and chemical structure of synthetic precursors (box) investigated in this study. (B) Crystal structure of HDM2:PMI complex (pdb 3EQS) and model of representative example of designer α -helical MOrPH (*i/i* + 10 peptide cyclization with SP8).

HDM2/X are implicated in the negative regulation of p53 activity and overexpression of these proteins has been linked to several malignancies.¹³ While dual inhibition of HDM2/X has emerged as a most promising strategy for anticancer therapy,¹⁴ small-molecule inhibitors of HDM2 typically fail to potently interfere with p53:HDMX interaction due to subtle differences in the p53 binding clefts of these protein homologs.¹⁵ These limitations make the development of dual HDM2/X inhibitors a topic of current interest.^{10c,16} HDM2 and HDMX bind to the N-terminal transactivation domain of p53 (p53₁₅₋₂₉), which upon complex formation adopts a well defined α -helix.¹⁷ Thus, in addition to its biomedical relevance, these structural features have made the p53:HDM2 interaction an ideal test bed to probe strategies for α -helix stabilization and mimicry.^{10c,11b,18}

Department of Chemistry, University of Rochester, Rochester, NY, USA.
E-mail: fasan@chem.rochester.edu; Tel: +1-585-2733504

† Electronic supplementary information (ESI) available: Experimental and synthetic procedures, additional inhibition curves. See DOI: 10.1039/c4cc01199f







The starting point for the design of our MORPH-based HDM2/X-targeting inhibitors was a linear 12-mer peptide isolated *via* phage display by Pazgier *et al.* (PMI: T¹SFAEYWNLSP¹²).¹⁹ PMI carries the triad of cofacial *i/i + 4/i + 7* amino acid residues known to be critical for p53 interaction with HDM2/X¹⁷ (*i.e.* Phe³, Trp⁷, and Leu¹⁰ corresponding to Phe¹⁹, Trp²³, and Leu²⁶ in p53, respectively), but inhibits these proteins with greater potency than a p53-derived peptide (IC₅₀: 30–40 nM *vs.* 200–300 nM, respectively).¹⁹ Upon inspection of the PMI–HDM2 complex structure (Fig. 1B),¹⁹ two solvent exposed residues, namely Thr¹ and Glu⁵, were identified as two equally viable side-chain attachment points for MORPH formation *via* substitution with *p*-acetyl-phenylalanine (pAcF) according to our oxime/AMA-mediated cyclization method (Fig. 1A).^{12c}

The C-terminal attachment site was chosen to lie after Ser¹¹ (changed to Ala to promote α -helix formation), as Pro¹² did not appear to establish significant contacts with the HDM2 surface.¹⁹ Analysis of models of the resulting peptide sequences, namely PMI-2 (GTSFA(pAcF)YWNLLA) and PMI-3 (G(pAcF)SFAEYWNLSP¹²), revealed that the distances between pAcF side-chain keto group and the C-terminal carbonyl group were about 13 and 16 Å, respectively. These distances matched the spacer distance (\sim 13 Å) furnished by one of our previously described synthetic linkers, called SP6^{12c} (Fig. 1A), based on an energy-minimized model of the compound (Fig. S1, ESI[†]). SP6 was thus selected as a first candidate for macrocyclization of the target peptide sequences PMI-2 and PMI-3. To examine the influence of the non-peptidic linker structure on the functional properties of the resulting MORPHs, a second linker reagent, SP8 (Fig. 1A), was prepared (see ESI[†] for details). SP8 satisfies the aforementioned distance requirements (Fig. S1, ESI[†]), but has higher flexibility compared to SP6 due to replacement of the triazole unit with an alkyl chain.

According to these design principles, macrocycles 3–5 and 7–9 were prepared *via* cyclization of PMI-2 or PMI-3 target sequences with SP6 or SP8 (see ESI[†] for details). 7–9 thus feature an *i/i + 10* side-chain-to-backbone connectivity, whereas in 3–5 the non-peptidic moiety bridges the *i* and *i + 6* residue. As controls, the same two peptide sequences were cyclized in the presence of the shorter reagent SP4 (Fig. 1A). Since the spacing distance provided by SP4 (\sim 8 Å, Fig. S1, ESI[†]) represents a mismatch with the target ones (13–16 Å), the resulting macrocycles (5 and 9) were intended to serve as negative control designs.

The ability of the designed macrocycles to disrupt the p53:HDM2/X interaction was assessed using a surface plasmon resonance (SPR) inhibition assay (Fig. S2, ESI[†]). Herein, biotinylated p53_(15–29) was immobilized on a streptavidin-coated biosensor chip and increasing concentrations of inhibitors were added to a fixed concentration of HDM2 or HDMX. Using this assay, half-maximal inhibitory concentrations (IC₅₀) were determined for the *i/i + 6* macrocycles 3–5 and compared to those obtained for the corresponding acyclic 2 and for a linear peptide (1) corresponding to the Hdm2/X-binding domain in p53. Gratifyingly, these studies revealed that both 3 and 4 possess improved inhibitory activity as compared to the acyclic counterpart 2 (Fig. S3, ESI[†]), exhibiting an approximately 2-fold lower IC₅₀ for HDMX (4) or for both HDM2 and HDMX (3) (Table 1). In contrast, SP4-based macrocycle 5 showed very weak inhibition (IC₅₀ \approx 10 μ M). Thus, these initial

Table 1 Sequence and inhibitory activity of peptides

Name	Sequence	HDM2 IC ₅₀ (nM)	HDMX IC ₅₀ (nM)
1 (p53 _{15–29})	SQETFSDLWKLLEN	920 \pm 65	1200 \pm 110
2	GTSFAYWNLLA	1510 \pm 95	7500 \pm 250
3	GTSFA-pAcF-YWNLLA 	870 \pm 53	4100 \pm 190
4	GTSFA-pAcF-YWNLLA 	1500 \pm 115	3500 \pm 95
5	GTSFA-pAcF-YWNLLA 	10 000 \pm 400	ND
6	GYSFAEYWNLAA	65 \pm 9	355 \pm 31
7	G-pAcF-SFAEYWNLAA 	475 \pm 37	910 \pm 105
8	G-pAcF-SFAEYWNLAA 	110 \pm 15	340 \pm 44
9	G-pAcF-SFAEYWNLAA 	> 50 000	> 50 000

data supported the ability of designer MORPHs 3 and 4 to accommodate the target α -helical motif, a conclusion supported also by the poor activity of 5. The latter indeed highlighted the deleterious effect of a mismatch between the length of the synthetic linker and the target side-chain...C-terminus bridging distance as anticipated. To our disappointment, however, both SP6- and SP8-based macrocycles were weaker inhibitors of HDM2/X compared to the wild-type p53 sequence (Table 1). This result can be rationalized based on the negative effect of replacing Glu5 with pAcF as required for macrocyclization. Indeed, in the crystal structure of the HDM2:PMI complex, Glu5 is found to form a hydrogen bond network with the neighboring Ser2 (Fig. S4, ESI[†]), which is likely to contribute to α -helix stabilization.¹⁶ This conclusion is supported also by the much higher inhibitory activity of the linear peptide 6 (*vs.* 2), in which the Ser2–Glu5 pair is preserved (Table 1).

To our delight, the *i/i + 10* macrocycles 7 and 8 exhibited significantly improved ability to disrupt p53 interaction with HDM2/X as compared to 3 and 4 (Fig. 2A and Fig. S3, ESI[†]). A notable effect of the type of synthetic linker on the binding properties of the corresponding MORPH was also apparent. Notably, the SP4-containing 9 was found to possess negligible inhibitory activity against HDM2 or HDMX (IC₅₀ > 50 μ M), confirming that cyclization *via* the ‘mismatching’ SP4 strongly disfavored adoption of the bioactive α -helical conformation by the embedded PMI-3 peptide sequence. In stark contrast, much higher inhibitory activity was observed in the presence of the ‘distance-matching’ SP6, leading to a compound with sub-micromolar IC₅₀ values for both protein homologues (Table 1). Interestingly, the simple replacement of the triazole unit in 7 with the alkyl chain in 8 led to a significant further improvement of inhibitory activity (3- to 4-fold) against both HDM2 (IC₅₀: 110 *vs.* 475 nM) and HDMX (IC₅₀: 340 *vs.* 910 nM). Intriguingly, the nature of the linker was found to have an effect also on the selectivity of the compounds against the two protein homologues. Indeed, while the unconstrained peptide 6 has stronger preference for HDM2 over HDMX, the macrocyclic counterparts, and in particular 7, behave more as dual, equipotent inhibitors (IC_{50(HDMX)}/IC_{50(HDM2)}} = 5.5 *vs.* 1.9, respectively). Overall, these}

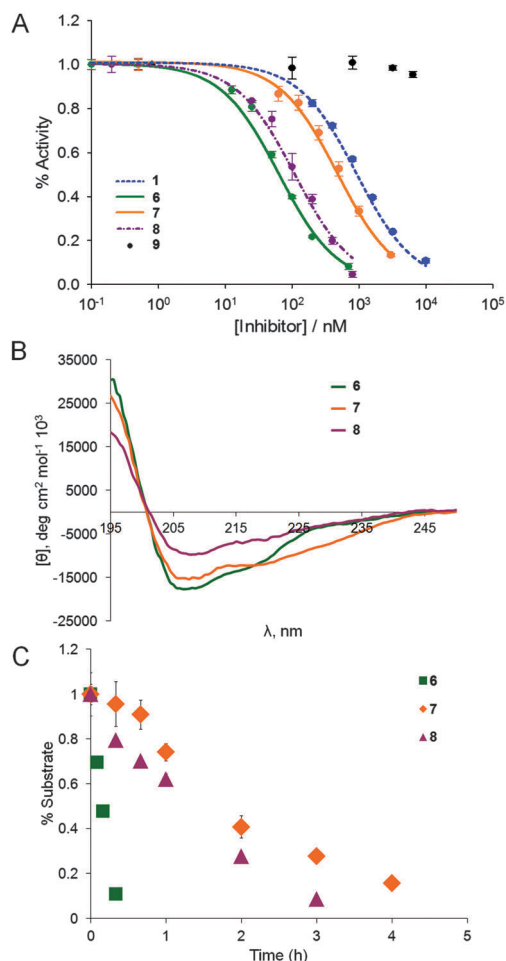


Fig. 2 Characterization data for representative compounds of Table 1. (A) SPR-based inhibition curves corresponding to disruption of HDM2/p53 interaction; (B) circular dichroism spectra measured in phosphate buffer (pH 7.0) with 40% TFE; (C) proteolytic stability tests in the presence of chymotrypsin ($1.0 \mu\text{g mL}^{-1}$) at room temperature.

studies led to the identification of macrocyclic inhibitors of the p53:HDM2/X interaction with much improved inhibitory activity compared to the wild-type p53 sequence, with the best compound, **8**, exhibiting a 8- and 3.5-fold lower IC_{50} value in the presence of HDM2 and HDMX, respectively.

To examine the impact of macrocyclization on the peptide conformational properties, circular dichroism (CD) analyses were performed on the most potent compounds **7** and **8** as well as on the linear peptide **6** as a control (Fig. 2B). Peptide **6** was found to display minima at 222 nm and 208 nm, which is consistent with the presence of an α -helical conformation. The α -helical content of the peptide was estimated to be about 31%. Cyclization of this sequence with SP6 (**7**) produced an increase in α -helicity (40%), whereas **8** showed a reduction in the α -helical content of the embedded peptide sequence (21%). The lack of a strict correlation between α -helicity and *in vitro* inhibitory activity has been observed for other types of p53:HDM2 inhibitors^{10c,11b} and it is not entirely unexpected considering that additional factors can affect the binding properties of these compounds, including potential interactions of the

linker moiety with the protein surface.¹⁶ Nevertheless, these experiments proved that a functional α -helical motif can be accommodated, and to some extent stabilized within the MORPH scaffolds, thereby providing a proof-of-principle validation of the design strategy outlined in Fig. 1B.

A potential benefit deriving from peptide macrocyclization is an enhancement in proteolytic stability. Despite its high potency *in vitro*, the linear peptide PMI was indeed found to be ineffective in cell-based assays in part due to rapid proteolysis.¹⁹ To assess this aspect, macrocycles **7** and **8**, along with the linear peptide **6**, were incubated in the presence of chymotrypsin (Fig. 2C). Not surprisingly, **6** was found to undergo rapid proteolytic degradation, with the original peptide becoming undetectable after only 30 minutes. In contrast, the macrocyclic peptides **7** and **8** survived up to 3 and 4 hour incubation with the protease, respectively, exhibiting a 10- to 15-fold longer half-life compared to the acyclic counterpart. These data clearly showed the beneficial effect of the intramolecular linkage in imparting these compounds with increased resistance against proteolysis. It was also interesting to note how the linker SP6 provided superior performance in terms of both α -helix stabilization and proteolytic resistance as compared to SP8, which may be linked to the reduced conformational flexibility of the former over the latter.

In summary, we have described the rational design of macrocyclic organo-peptide hybrids that can effectively accommodate and, to a certain extent, stabilize an α -helical protein binding motif. While a common approach in the area of α -helix stabilization has involved the use of inter-side-chain covalent linkages,⁴ this work represents, to the best of our knowledge, the first example of exploiting side-chain-to-tail peptide cyclization for this purpose. Using this strategy, submicromolar inhibitors of the p53:HDM2 interaction which display dual specificity against the HDMX isoform as well as increased proteolytic stability were obtained. Another intriguing aspect concerns the influence of the non-peptidic moiety in modulating the functional, conformational, and stability properties of these α -helical MORPHs. These findings lay the ground for future efforts directed at leveraging this feature to further optimize these compounds and exploring the potential of the present approach toward disrupting other α -helix-mediated protein-protein interactions.

This work was supported by the U.S. National Science Foundation grant CHE-1112342. J.M.S. acknowledges the NSF GRF program for financial support. MS instrumentation was supported by the U.S. National Science Foundation grants CHE-0840410 and CHE-0946653.

Notes and references

- (a) J. A. Wells and C. L. McClendon, *Nature*, 2007, **450**, 1001; (b) M. C. Smith and J. E. Gestwicki, *Expert Rev. Mol. Med.*, 2012, **14**, e16.
- (a) J. A. Robinson, S. Demarco, F. Gombert, K. Moehle and D. Obrecht, *Drug Discovery Today*, 2008, **13**, 944; (b) L. R. Whitby and D. L. Boger, *Acc. Chem. Res.*, 2012, **45**, 1698.
- A. L. Jochim and P. S. Arora, *Mol. Biosyst.*, 2009, **5**, 924.
- L. K. Henchey, A. L. Jochim and P. S. Arora, *Curr. Opin. Chem. Biol.*, 2008, **12**, 692.
- D. Wang, W. Liao and P. S. Arora, *Angew. Chem., Int. Ed.*, 2005, **44**, 6525.

- 6 D. Y. Jackson, D. S. King, J. Chmielewski, S. Singh and P. G. Schultz, *J. Am. Chem. Soc.*, 1991, **113**, 9391.
- 7 G. Osapay and J. W. Taylor, *J. Am. Chem. Soc.*, 1992, **114**, 6966.
- 8 F. M. Brunel and P. E. Dawson, *Chem. Commun.*, 2005, 2552.
- 9 (a) M. Scrima, A. Le Chevalier-Isaad, P. Rovero, A. M. Papini, M. Chorev and A. M. D'Ursi, *Eur. J. Org. Chem.*, 2010, 446; (b) S. A. Kawamoto, A. Coleska, X. Ran, H. Yi, C. Y. Yang and S. Wang, *J. Med. Chem.*, 2012, **55**, 1137.
- 10 (a) H. E. Blackwell and R. H. Grubbs, *Angew. Chem., Int. Ed.*, 1998, **37**, 3281; (b) C. E. Schafmeister, J. Po and G. L. Verdine, *J. Am. Chem. Soc.*, 2000, **122**, 5891; (c) F. Bernal, M. Wade, M. Godes, T. N. Davis, D. G. Whitehead, A. L. Kung, G. M. Wahl and L. D. Walensky, *Cancer Cell*, 2010, **18**, 411.
- 11 (a) F. Z. Zhang, O. Sadovskii, S. J. Xin and G. A. Woolley, *J. Am. Chem. Soc.*, 2007, **129**, 14154; (b) A. Muppidi, Z. Wang, X. Li, J. Chen and Q. Lin, *Chem. Commun.*, 2011, **47**, 9396; (c) H. Jo, N. Meinhardt, Y. B. Wu, S. Kulkarni, X. Z. Hu, K. E. Low, P. L. Davies, W. F. DeGrado and D. C. Greenbaum, *J. Am. Chem. Soc.*, 2012, **134**, 17704; (d) A. M. Spokoiny, Y. Zou, J. J. Ling, H. Yu, Y. S. Lin and B. L. Pentelute, *J. Am. Chem. Soc.*, 2013, **135**, 5946.
- 12 (a) J. M. Smith, F. Vitali, S. A. Archer and R. Fasan, *Angew. Chem., Int. Ed.*, 2011, **50**, 5075; (b) M. Satyanarayana, F. Vitali, J. R. Frost and R. Fasan, *Chem. Commun.*, 2012, **48**, 1461; (c) J. R. Frost, F. Vitali, N. T. Jacob, M. D. Brown and R. Fasan, *ChemBioChem*, 2013, **14**, 147.
- 13 (a) J. C. Marine, M. A. Dyer and A. G. Jochemsen, *J. Cell Sci.*, 2007, **120**, 371; (b) G. M. Wahl and M. Wade, *Mol. Cancer Res.*, 2009, **7**, 1.
- 14 (a) B. Hu, D. M. Gilkes, B. Farooqi, S. M. Sebti and J. Chen, *J. Biol. Chem.*, 2006, **281**, 33030; (b) M. Wade, E. T. Wong, M. Tang, J. M. Stommel and G. M. Wahl, *J. Biol. Chem.*, 2006, **281**, 33036.
- 15 G. M. Popowicz, A. Czarna, U. Rothweiler, A. Szwagierczak, M. Krajewski, L. Weber and T. A. Holak, *Cell Cycle*, 2007, **6**, 2386.
- 16 C. J. Brown, S. T. Quah, J. Jong, A. M. Goh, P. C. Chiam, K. H. Khoo, M. L. Choong, M. A. Lee, L. Yurlova, K. Zolghadr, T. L. Joseph, C. S. Verma and D. P. Lane, *ACS Chem. Biol.*, 2013, **8**, 506.
- 17 (a) P. H. Kussie, S. Gorina, V. Marechal, B. Elenbaas, J. Moreau, A. J. Levine and N. P. Pavletich, *Science*, 1996, **274**, 948; (b) G. M. Popowicz, A. Czarna and T. A. Holak, *Cell Cycle*, 2008, **7**, 2441.
- 18 (a) R. Fasan, R. L. Dias, K. Moehle, O. Zerbe, J. W. Vrijbloed, D. Obrecht and J. A. Robinson, *Angew. Chem., Int. Ed.*, 2004, **43**, 2109; (b) J. A. Kritzer, J. D. Lear, M. E. Hodsdon and A. Schepartz, *J. Am. Chem. Soc.*, 2004, **126**, 9468; (c) H. Yin, G. I. Lee, H. S. Park, G. A. Payne, J. M. Rodriguez, S. M. Sebti and A. D. Hamilton, *Angew. Chem., Int. Ed.*, 2005, **44**, 2704; (d) R. Fasan, R. L. Dias, K. Moehle, O. Zerbe, D. Obrecht, P. R. Mittl, M. G. Grutter and J. A. Robinson, *ChemBioChem*, 2006, **7**, 515; (e) T. Hara, S. R. Durell, M. C. Myers and D. H. Appella, *J. Am. Chem. Soc.*, 2006, **128**, 1995; (f) J. K. Murray and S. H. Gellman, *Biopolymers*, 2007, **88**, 657; (g) C. Li, M. Liu, J. Monbo, G. Zou, W. Yuan, D. Zella, W. Y. Lu and W. Lu, *J. Am. Chem. Soc.*, 2008, **130**, 13546; (h) L. K. Henchey, J. R. Porter, I. Ghosh and P. S. Arora, *ChemBioChem*, 2010, **11**, 2104.
- 19 M. Pazgier, M. Liu, G. Zou, W. Yuan, C. Li, J. Li, J. Monbo, D. Zella, S. G. Tarasov and W. Lu, *Proc. Natl. Acad. Sci. U. S. A.*, 2009, **106**, 4665.

Supplemental Information for

**Macrocyclic peptides inhibit the interaction of p53 with
HDM2 and HDMX by accommodating a functional α -helix
motif**

Jessica M. Smith, John R. Frost, and Rudi Fasan*

Department of Chemistry, University of Rochester, Rochester, New York 14627, USA.

*Corresponding author: fasan@chem.rochester.edu

<u>Index</u>	<u>Page</u>
Figure S1-S4	S2-S5
Experimental procedures	S6-S8
Synthetic procedures	S9-S10
References	S11

Figure S1. Energy minimized models of the organic linkers SP6 (A), SP8 (B), and SP4 (C) illustrating the near-maximal spanning distance between the two ligation points within the target peptide. The side-chain attachment site is mimicked by an acetophenone moiety, whereas the C-terminal attachment site is mimicked by an acetyl moiety. The distance between the carbon atoms of the oxime and amide groups is indicated.

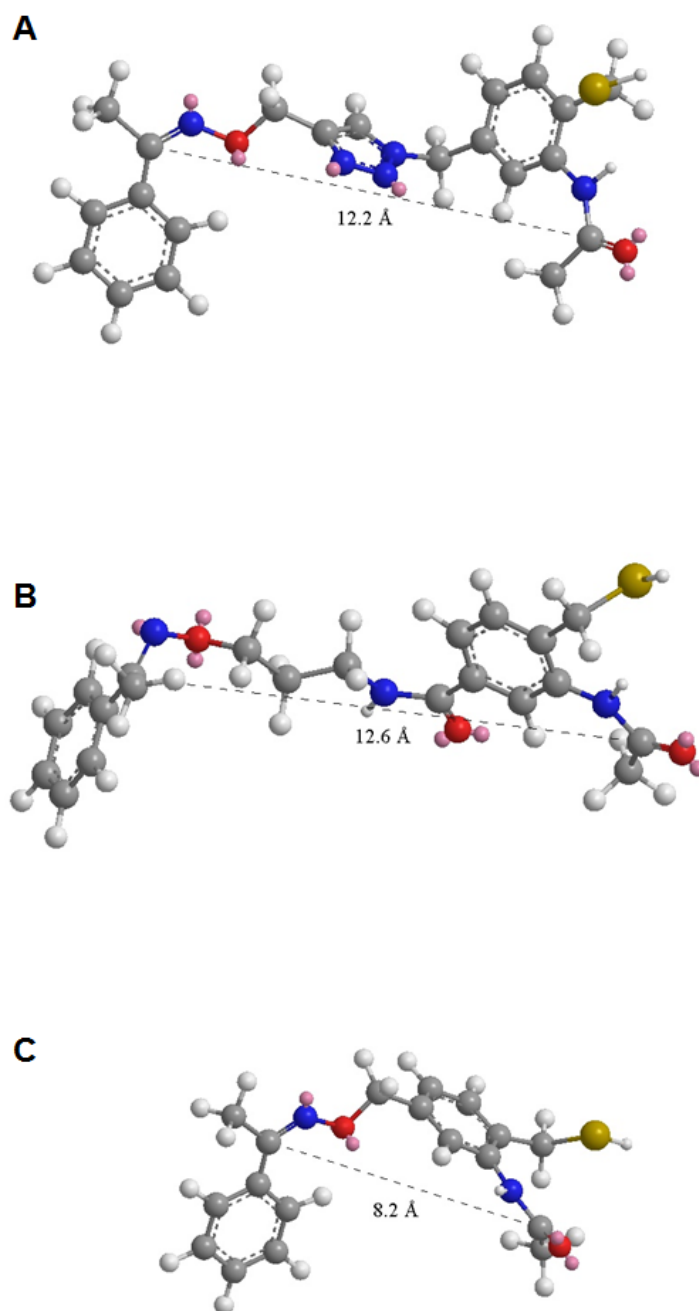


Figure S2. Biacore sensogram response curves of HDM2 binding to immobilized p53 peptide in the presence of varying concentrations of peptide **1** (p53₁₅₋₂₉).

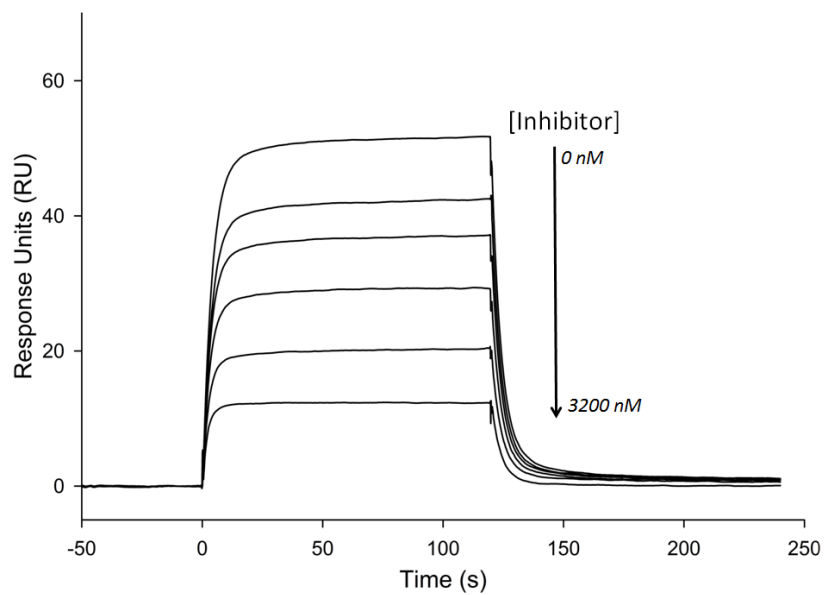


Figure S3. Concentration dependent inhibition of HDM2:p53₁₅₋₂₉ and HDMX:p53₁₅₋₂₉ complex formation by MOrPHs and linear peptide controls. A) Inhibition of HDM2 with peptides **2**, **3**, **4**, and **5**; B) inhibition of HDMX with peptides **1**, **6**, **7**, **8**, and **9**; C) inhibition of HDMX with peptides **2**, **3**, and **4**.

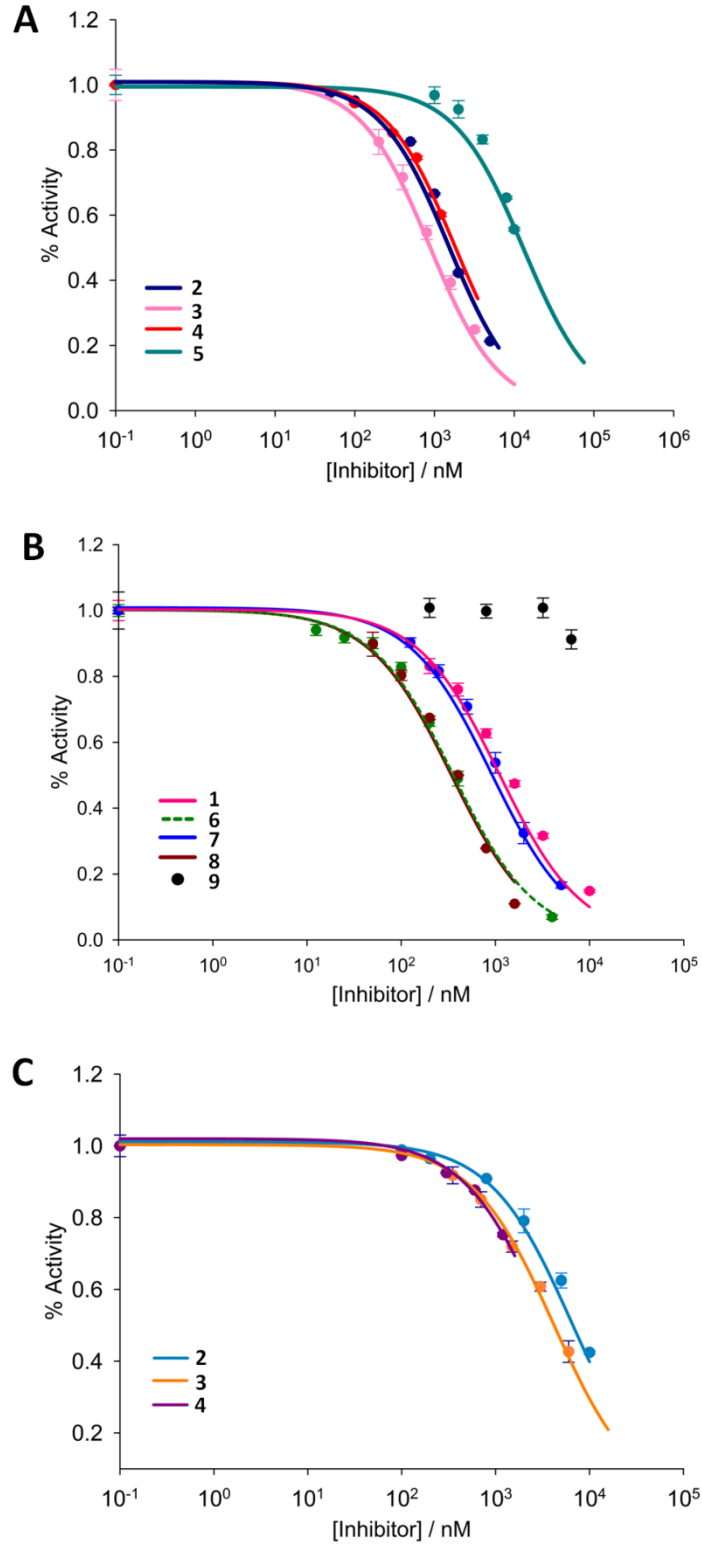
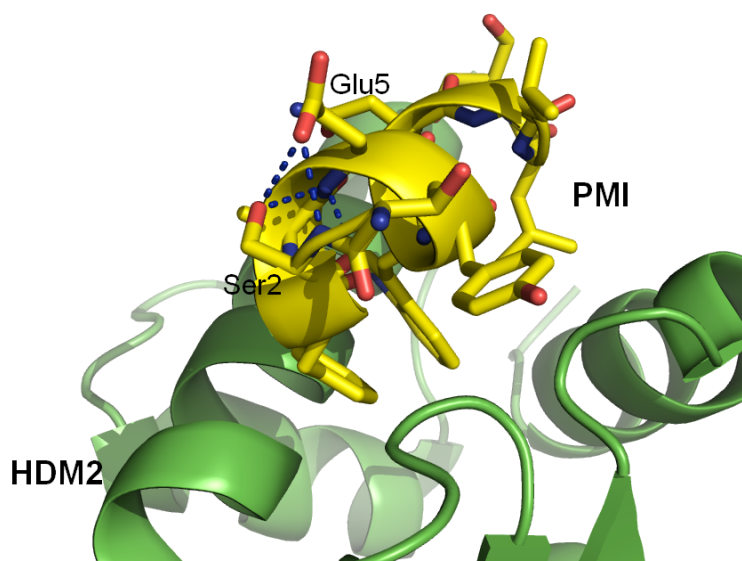


Figure S4. H-bond network between Glu5 side-chain carboxylic group and Ser2 amide NH and side-chain hydroxy group in the PMI peptide bound to HDM2 (pdb 3EQS).¹



EXPERIMENTAL PROCEDURES

Cloning, Expression, and Purification of HMD2 and HMDX proteins. Genes encoding for the p53-binding domain of human HDM2 (residues 1-109) and human HDMX (residues 1-109) were cloned into a pET22 vector (Novagen). The template for PCR amplification of the HDM2 gene was plasmid pGEX-4T MDM2 WT (AddGene # 16237).² A template for PCR amplification of the HDMX gene was kindly provided by Prof. Mike Dyer in the Division of Developmental Biology at the St. Jude Children's Research Hospital (Memphis, TN). In the final plasmid constructs (pET22-HDM2-YFP-His and pET22-HDMX-YFP-His), the HDM2/X protein was C-terminally fused to Yellow Fluorescent Protein (YFP) containing a C-terminal His tag. Fusion to the YFP protein was found to improve the solubility and stability of the protein constructs. To isolate the HDM2-YFP and HDMX-YFP fusion proteins, pET22-HDM2-YFP-His and pET22-HDMX-YFP-His plasmids were each transformed into BL21(DE3) cells followed by plating and overnight growth in LB medium containing ampicillin (50 mg L⁻¹). The overnight cultures were used to inoculate a 500 mL LB culture (ampicillin at 50 mg L⁻¹), which was induced with 0.5 mM IPTG at OD₆₀₀ ~ 0.6, and incubated for 16 hours at 27 °C. Cells were harvested by centrifugation and lysed by sonication. The clarified lysate was loaded onto a Ni-NTA affinity column and the protein was eluted with 50 mM Tris, 150 mM NaCl, 300 mM imidazole (pH 7.4). After buffer exchange with potassium phosphate 50 mM, NaCl 150 mM buffer (pH 7.5), aliquots of the protein solutions were stored at -80°C. Protein concentration was determined using the extinction coefficient at 280 nm (ϵ_{280}) calculated based on the protein primary sequence. The identity of the isolated protein was confirmed by MALDI-TOF and SDS-PAGE.

Cloning, Expression, and Purification of PMI-2 and PMI-3 Containing Biosynthetic Precursors.

The protein precursors containing the target peptide sequence PMI-3 (GTSFA(pAcF)YWNLLA) and PMI-2 (G(pAcF)SFAEYWNLLA) followed by *Mxe* GyrA(N198A) intein and a C-terminal His tag were prepared as follows. First, genes that encode for these peptide sequences (an amber stop codon, TAG, is used for incorporation of pAcF) fused to the GyrA gene were generated by PCR using the pET22b-based plasmid pMG-G8T³ as template, forward primers PMI_for1 5'-GCGATTGGAACCTGCTGGCGTGCATCACGG-GAGATGCACTAGT-3' and PMI_for2 5'-CTAGACATAT-GGGCTAGAGCTTCGCGGAATATTGGAACCTGCTGGCGTGCAT-3', and the reverse primer T7_terminator 5'-GCTAGTTATTGCTCAGCGGTGGC-3'. The resulting PCR products (~ 0.75 Kbp) were cloned into pET22 plasmid (Novagen) using *Nde* I and *Xho* I restriction enzymes, to produce the plasmids pPMI-2-GyrA and pPMI-3-GyrA. In these constructs, the gene encoding for the biosynthetic precursor protein is under the control of an IPTG-inducible T7 promoter. The precursor proteins were expressed by co-transforming pPMI-2-GyrA (or pPMI-3-GyrA) and a pEVOL-based vector

encoding for a reported *Mj* tRNA_{CUA} / aminoacyl-tRNA synthetase pair⁴ for amber stop codon suppression with *para*-acetylphenylalanine (pAcF), into BL21(DE3) *E. coli* cells. Protein expression was carried out as described.³ After expression, the proteins were purified Ni-affinity chromatography as described above. The identity of the isolated protein was confirmed by MALDI-TOF and SDS-PAGE. MS analysis indicated complete cleavage of the initial methionine in the purified proteins.

Synthesis and Purification of PMI-based MOrPHs. The PMI-2 and PMI-3-based MOrPHs were prepared by large scale macrocyclization reactions between precursor protein PMI-2-GyrA (or PMI-3-GyrA) and the appropriate synthetic precursor (SP6, SP8, or SP4). In addition to providing the desired compounds, this approach was chosen (over solid-phase peptide synthesis) to demonstrate the scalability of our catalyst-free chemobiosynthetic method for MOrPH synthesis.³ In a typical reaction, the protein (200 μ M in potassium phosphate 50 mM, NaCl 150 mM buffer (pH 7.5)) was mixed with 10 mM synthetic precursor and 10 mM TCEP (total volume: 6 mL). After 30 hrs, the pH of the reaction mixture was adjusted to 8.5 and incubated with iodoacetamide (15 mM) for 1 hour to cap the free thiol group. The reaction was centrifuged at 4000 x g for 2 minutes, after which the supernatant (*a*) was separated from the pellet. The pellet was resuspended in 20% acetonitrile/H₂O by vortexing for several minutes to dissolve the MOrPH product, then centrifuged at 4000 x g for 2 minutes to provide supernatant (*b*). The supernatants (*a* and *b*) were combined and applied to a solid-phase extraction C₁₈ column pre-washed with 10 column volumes (CV) MeOH, 10 CV acetonitrile, and 10 CV water. The macrocyclic product was eluted using a gradient of acetonitrile in water from 10% to 80%. The eluted MOrPH was further purified by HPLC using a GraceSmart RP C18 column (250 x 4.6mm, 5 μ m) maintained at 25°C, a flow rate of 0.9 mL/min, a binary mobile phase system consisting of A: water + 0.1% TFA and B: acetonitrile + 0.1% TFA, and a linear gradient from 10% to 90% solvent B (12 min). The identity of the isolated MOrPH was confirmed by LC-MS and MS/MS. Masses for all MOrPH products are listed in Table S1.

Table S1. Calculated and observed masses of MOrPH ligands

Peptide	Mass Calc. [M+H] ⁺	Mass Obs. [M+H] ⁺
3	1718.5	1719.1
4	1708.9	1708.4
5	1637.9	1637.5
7	1746.4	1746.2
8	1736.9	1737.3
9	1608.8*	1608.5*

* denotes free thiol (no acetamide alkylation)

Inhibition Assays. The surface plasmon resonance (SPR)-based inhibition assays were performed using a BIAcore T100 instrument. A HDM2/X binding surface was first generated by immobilizing ~500 RU of a biotinylated p53 peptide (biotin-SGSG-p53₁₅₋₂₉) on a streptavidin-coated biosensor chip (SA chip, GE Healthcare). Running buffer and sample buffer contained 10 mM HEPES buffer, pH 7.4 with 150 mM NaCl, 3 mM EDTA and 0.05% v/v Tween 20. For the inhibition studies, increasing concentrations of inhibitor were added to a fixed concentration (150 nM) of purified HDM2-YFP or HDMX-YFP and the mixture was injected over the functionalized surface. With increasing concentrations of the inhibitor, binding of HDM2 (or HDMX) to the surface is inhibited, leading to a decrease in biosensor response. HDM2/HDMX plus inhibitor samples were injected at a rate of 30 uL/min over a 2 minute interval (Figure S4) by a 2 minute dissociation period and a 10-second regeneration step using 10 mM HCl. The chip was allowed to re-equilibrate for 1 minute between runs in running buffer. Specific binding curves for each concentration of inhibitor were obtained by subtracting the response in the reference surface from the response in the p53-coated surface. Response values were calculated by averaging the last 10 s of each sample injection. The data was analyzed with SigmaPlot 12.5 software and the sigmoidal plots fitted to the Hill equation for a one site competitive binding to derive IC₅₀ values (Figure S2). Reported IC₅₀ average values and standard deviations were derived from at least two independent experiments.

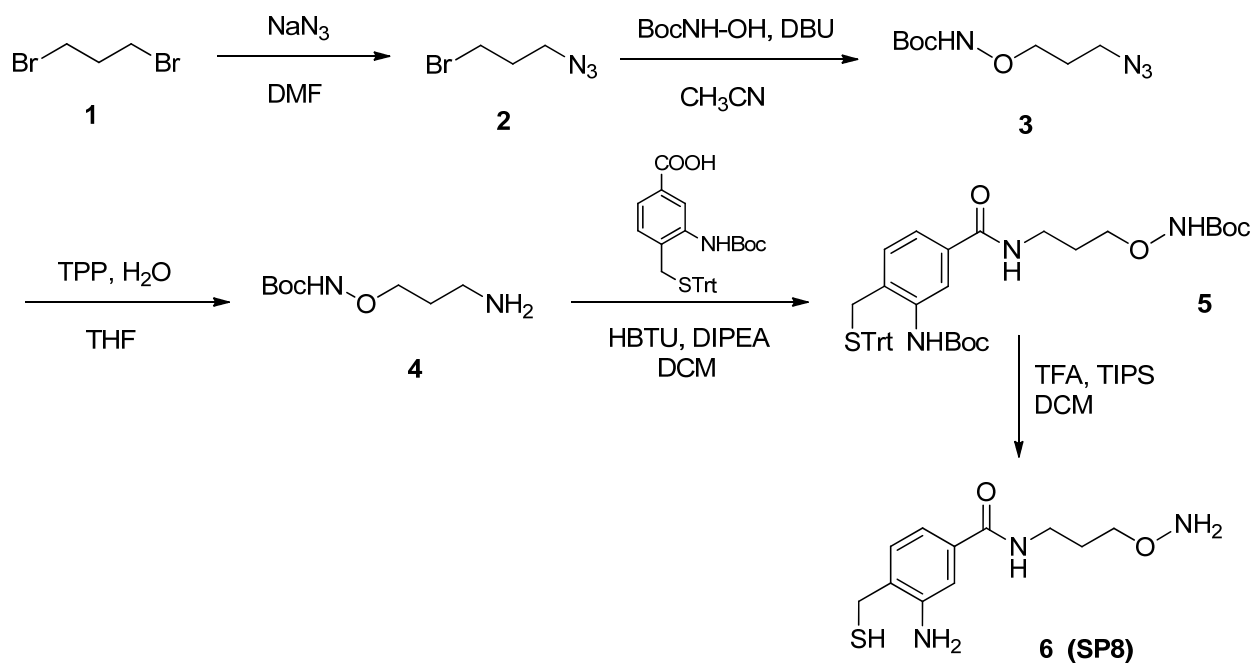
Circular Dichroism Studies. CD spectra were recorded with a JASCO J-710 CD spectropolarimeter using a 0.1 cm path length cuvette at room temperature. The purified peptides were dissolved in 5 mM potassium phosphate buffer (pH 7.0) containing 40% trifluoroethanol to a final concentration of 20-50 μM. Spectra were averaged over 2 scans recorded from 195 to 250 nm wavelength range with a speed of 10 nm/min, a response time of 1.0 s, and a resolution of 0.5 nm. The bandwidth was set to 2.0 nm and the sensitivity of the spectrometer set to 100 mdeg. The mean residue ellipticity was plotted vs. wavelength and the helical content of each peptide derived based on the following formula: $[\theta]_{222}/[40000 \times (n - 4)/n]$ where n = number of peptide bonds.⁵

Analysis of Proteolytic Resistance. Each peptide (10 μM) was dissolved in 50 mM potassium phosphate buffer (pH 7.5) containing 150 mM NaCl and 10% DMSO. Chymotrypsin (Sigma-Aldrich) was added to a final concentration of 1.0 μg / mL and incubated at room temperature. At each time point, a 50 μL aliquot of the mixture was removed, quenched by TFA addition (5 μL) followed by HPLC analysis. Peptide cleavage was monitored based on the decrease of the peak area corresponding to the integer peptide. Experiments were performed at least in duplicate. HPLC analyses were carried out using a GraceSmart RP C18 column (250 x 4.6mm, 5 μm) maintained at 25°C, a flow rate of 0.9 mL/min, a binary mobile phase system consisting of A: water + 0.1% TFA and B: acetonitrile + 0.1% TFA, and a linear gradient from 10% to 90% solvent B in 12 min.

SYNTHETIC PROCEDURES

Synthesis of SP6 and SP4. Synthetic precursors SP6 and SP4 were synthesized as described previously.³

Synthesis of SP8.



1-azido-3-bromopropane (2): A solution of 1,3-dibromopropane (1) (4.0 g, 19.8 mmol) in dry DMF (30 mL) was placed under argon. Sodium azide (1.16 g, 17.8 mmol) was added and the reaction stirred at 50 °C for 16 hours. The reaction was cooled to room temperature and extracted from ice-cold water with ethyl acetate (3 x 20 mL). The combined organic layers were washed with brine, dried over Na₂SO₄, and concentrated *in vacuo* to yield a yellow oil. The crude product was purified by silica gel flash chromatography (100% hexanes) to yield 2 (1.62 g, 50%) as a clear oil. ¹H NMR (400 MHz, CDCl₃): δ 2.06-2.12 (m, 2 H), 3.47-3.51 (m, 4 H).

tert-butyl (3-azidopropoxy)carbamate (3): 1-azido-3-bromopropane (2) (0.73 g, 4.45 mmol) was dissolved in acetonitrile (14 mL). DBU (1.33 mL, 8.91 mmol) and *N*-Boc-hydroxylamine (0.889 g, 6.68 mmol) were added to the solution, which was placed under argon and connected to a reflux condenser. The reaction was heated to 50 °C. After 20 h, water (35 mL) was added and the product was extracted with ethyl acetate (3 x 20 mL). The combined organic layers were washed with brine, dried over Na₂SO₄, and concentrated *in vacuo*. The crude product was then purified by silica gel flash chromatography with hexanes : ethyl acetate (95:5) to afford 3 as a clear oil (0.8 g, 83%). ¹H NMR (400 MHz, CDCl₃): δ 1.48 (s, 9 H), 1.88-1.91 (m, 2 H), 3.45 (t, 2 H, J = 6.6), 3.93 (t, 2 H, J = 6.0), 7.11 (br, 1 H).

tert-butyl (3-aminopropoxy)carbamate (4): Triphenylphosphine (1.16 g, 4.44 mmol) was added to a solution of *t*-butyl (3-azidopropoxy)carbamate (**3**) (0.8 g, 3.70 mmol) in THF (17 mL) and water (0.3 mL). The reaction mixture was stirred at room temperature for 12 hours. THF was then removed under reduced pressure and the crude product was purified by silica gel flash chromatography with dichloromethane : methanol (80:20) to yield **4** as a yellow oil (0.51 g, 71%). ¹H NMR (500 MHz, CDCl₃): δ 1.47 (s, 9 H), 1.77-1.81 (m, 2 H), 2.88 (t, 2 H, J = 6.5), 3.95 (t, 2 H, J = 5.5). ¹³C NMR (125 MHz, CDCl₃): δ 28.23, 30.50, 39.02, 74.89, 81.69, 157.1. MS (ESI) calcd for C₈H₁₈N₂O₃ [M+H]⁺ *m/z*: 191.24; found: 191.55.

tert-butyl(5-((3-(((tert-butoxycarbonyl)amino)oxy)propyl)carbamoyl)-2-((tritylthio)methyl)phenyl)carbamate (5): 3-((tert-butoxycarbonyl)amino)-4-((tritylthio)methyl)benzoic acid (0.677 g, 1.31 mmol) was dissolved in dichloromethane (15 mL) and the solution was added with *tert*-butyl-3-aminopropoxycarbamate (**4**) (0.25 g, 1.31 mmol), HBTU (0.745 g, 1.96 mmol), and DIPEA (0.55 mL, 3.15 mmol) under argon. The reaction mixture was stirred at room temperature for 3 hours, after which it was diluted with water and extracted with dichloromethane (3 x 40 mL). The organic layers were concentrated under reduced pressure to afford a crude residue, which was then purified by silica gel flash chromatography using hexanes : ethyl acetate (70:30) to yield **5** (0.658 g, 72%). ¹H NMR (400 MHz, CDCl₃): δ 1.45 (s, 9 H), 1.52 (s, 9 H), 1.85-1.90 (m, 2 H), 3.18 (s, 2 H), 3.56-3.61 (m, 2 H), 3.98 (t, 2 H, J = 5.6), 7.14 (d, 1 H, J = 8.0), 7.22-7.26 (m, 3 H), 7.30-7.34 (m, 6 H), 7.48-7.52 (m, 7 H), 8.18 (s, 1 H).

3-amino-N-(3-(aminooxy)propyl)-4-(mercaptomethyl)benzamide (6): *tert*-butyl (5-((3-(((tert-butoxycarbonyl)amino)oxy)propyl)carbamoyl)-2-((tritylthio)methyl)phenyl)carbamate (**5**) (0.48 g, 0.69 mmol) was dissolved in dichloromethane (7.5 mL) under argon at 0 °C. Triisopropylsilane (0.36 mL, 1.75 mmol) was added, followed by TFA (1.6 mL, dropwise). The reaction was stirred for 30 minutes at 0 °C. Volatiles were then removed *in vacuo* and the yellow residue placed under high vacuum over night. The product was triturated with ice-cold hexanes and dried *in vacuo* to yield SP8 as a solid (0.18 g, quant.). ¹H NMR (500 MHz, d₄-MeOD): δ 1.95-2.01 (m, 2 H), 3.48 (t, J = 6.8, 2 H), 3.72 (s, 2 H), 4.11 (t, 2 H, J = 6.0), 7.09 (d, J = 8.0, 1 H), 7.13 (d, J = 8.0, 1 H), 7.23 (s, 1 H). ¹³C NMR (125 MHz, d₄-MeOD): δ 29.14, 37.34, 40.14, 74.16, 116.3, 116.6, 117.8, 126.5, 132.7, 135.9, 170.5. MS (ESI) calcd for C₁₁H₁₇N₃O₂S [M+H]⁺ *m/z*: 256.34; found: 255.92.

REFERENCES

- 1 Pazgier, M.; Liu, M.; Zou, G.; Yuan, W.; Li, C.; Li, J.; Monbo, J.; Zella, D.; Tarasov, S. G.; Lu, W., *Proc. Natl. Acad. Sci. USA*, 2009, **106**, 4665.
- 2 Zhou, B. P.; Liao, Y.; Xia, W.; Zou, Y.; Spohn, B.; Hung, M. C., *Nat Cell Biol*, 2001, **3**, 973.
- 3 Frost, J. R.; Vitali, F.; Jacob, N. T.; Brown, M. D.; Fasan, R., *Chembiochem*, 2013, **14**, 147.
- 4 Wang, L.; Zhang, Z.; Brock, A.; Schultz, P. G., *Proc. Natl. Acad. Sci. USA*, 2003, **100**, 56.
- 5 Johnson, W. C., Jr.; Tinoco, I., Jr., *J Am Chem Soc*, 1972, **94**, 4389.